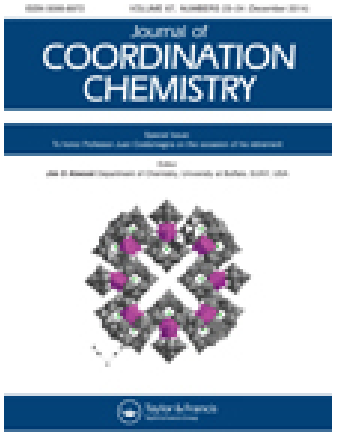

Journal of Coordination Chemistry
Publication details, including instructions for authors and subscription information:
http://www.tandfonline.com/loi/gcoo20

3-Pyridylacetonitrile-ligated 11-vertex rhodathiaboranes: synthesis, characterization, and X-ray crystal structure

B. Calvo[a], M. Keß[a], R. Macias[a], R. Sancho[a], F.J. Lahoz[a] & L.A. Oro[ab]

[a] Departamento de Química Inorgánica, Instituto de Síntesis Química y Catálisis Homogénea (ISQCH), Universidad de Zaragoza - CSIC, Zaragoza, Spain

[b] Center of Research Excellence in Refining & Petrochemicals, King Fahd University of Petroleum & Minerals, Dhahran, Saudi Arabia

Accepted author version posted online: 01 Sep 2014.Published online: 25 Sep 2014.

To cite this article: B. Calvo, M. Keß, R. Macias, R. Sancho, F.J. Lahoz & L.A. Oro (2014) 3-Pyridylacetonitrile-ligated 11-vertex rhodathiaboranes: synthesis, characterization, and X-ray crystal structure, Journal of Coordination Chemistry, 67:23-24, 4016-4027, DOI: 10.1080/00958972.2014.959004

To link to this article: http://dx.doi.org/10.1080/00958972.2014.959004

Journal of Coordination Chemistry, 2014
Vol. 67, Nos. 23–24, 4016–4027, http://dx.doi.org/10.1080/00958972.2014.959004

3-Pyridylacetonitrile-ligated 11-vertex rhodathiaboranes: synthesis, characterization, and X-ray crystal structure

B. CALVO†, M. KEß†, R. MACIAS*†, R. SANCHO†, F.J. LAHOZ† and L.A. ORO*†‡

†Departamento de Química Inorgánica, Instituto de Síntesis Química y Catálisis Homogénea (ISQCH), Universidad de Zaragoza – CSIC, Zaragoza, Spain
‡Center of Research Excellence in Refining & Petrochemicals, King Fahd University of Petroleum & Minerals, Dhahran, Saudi Arabia

(*Received 5 June 2014; accepted 21 July 2014*)

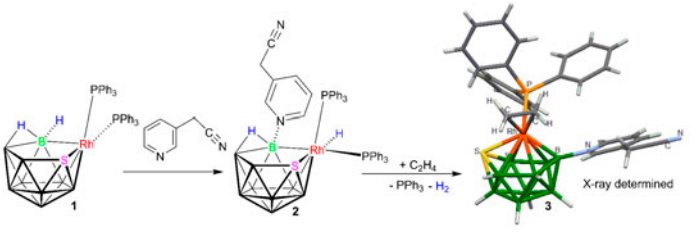

The reaction between the 11-vertex rhodathiaborane [8,8-$(PPh_3)_2$-*nido*-8,7-$RhSB_9H_{10}$] (**1**) and 3-pyridylacetonitrile affords the hydrorhodathiaborane [8,8,8-$(PPh_3)_2$H-9-(3-Py-CH_2CN)-*nido*-8,7-$RhSB_9H_9$] (**2**) in good yield. Treatment of this cluster with ethylene leads to the formation of red, [1,1-$(PPh_3)(\eta^2$-$C_2H_4)$-3-(3-Py-CH_2CN)-*closo*-1,2-$RhSB_9H_8$] (**3**). Both 11-vertex polyhedral boron-based clusters have been characterized by multielement NMR spectroscopy. In addition, (**3**) has been analyzed by single-crystal X-ray diffraction analysis and is only the second ethylene-ligated metalla-heteroborane to be characterized in the solid state. The molecular structure of this cluster is based on an octadecahedron. In the crystal lattice, the individual clusters form layers supported by short edge-to-face π-interactions between the phenyl rings of neighboring molecules.

Keywords: Polyhedral clusters; Rhodathiaboranes; Ethylene; Boron; Rhodium

1. Introduction

Metallaheteroboranes are polyhedral boron-based clusters that feature M–B, E–B, and B–B bonds, where M and E are metallic and *p*-block elements, respectively. Metallacarboranes, where E = C, form the largest group of metallaheteroboranes for which a systematic study of their reaction chemistry has been carried out [1–13]. In contrast, the reaction chemistry of other metallaheteroboranes is poorly developed [14–20].

*Corresponding authors. Email: rmacias@unizar.es (R. Macias); oro@unizar.es (L.A. Oro)
Dedicated to Prof. Juan Costamagna, a superb mentor of a number of Latin American scientists working on coordination chemistry.

The high-yield synthesis of the 11-vertex [8,8-$(PPh_3)_2$-*nido*-8,7-$RhSB_9H_{10}$] (**1**) [21] from the reaction of Wilkinson's compound with $CsSB_9H_{12}$ has allowed the development of a systematic chemistry based on this cluster. During our research dealing with **1**, we have discovered that the reaction with pyridine affords the hydridorhodathiaborane, [8,8,8-$(PPh_3)_2$H-9-(NC_5H_5)-*nido*-8,7-$RhSB_9H_9$]. This 11-vertex cluster exhibits a remarkable structural *nido*-to-*closo* flexibility that has led to a rich reaction chemistry that embraces the following: (i) *nido*-to-*closo* dehydrogenations [22], (ii) dihydrogen-promoted *closo*-to-*nido* transformations [23, 24], (iii) oxidative addition of *sp* C–H bonds [25], (iv) proton-assisted H_2 activation [26], and (v) catalysis of hydrogenation and isomerization of olefins [23] (scheme 1).

Based on these results, and in order to modify the *exo*-polyhedral surface of the clusters, we report the reaction of the parent rhodathiaborane **1** with 3-pyridylacetonitrile. The

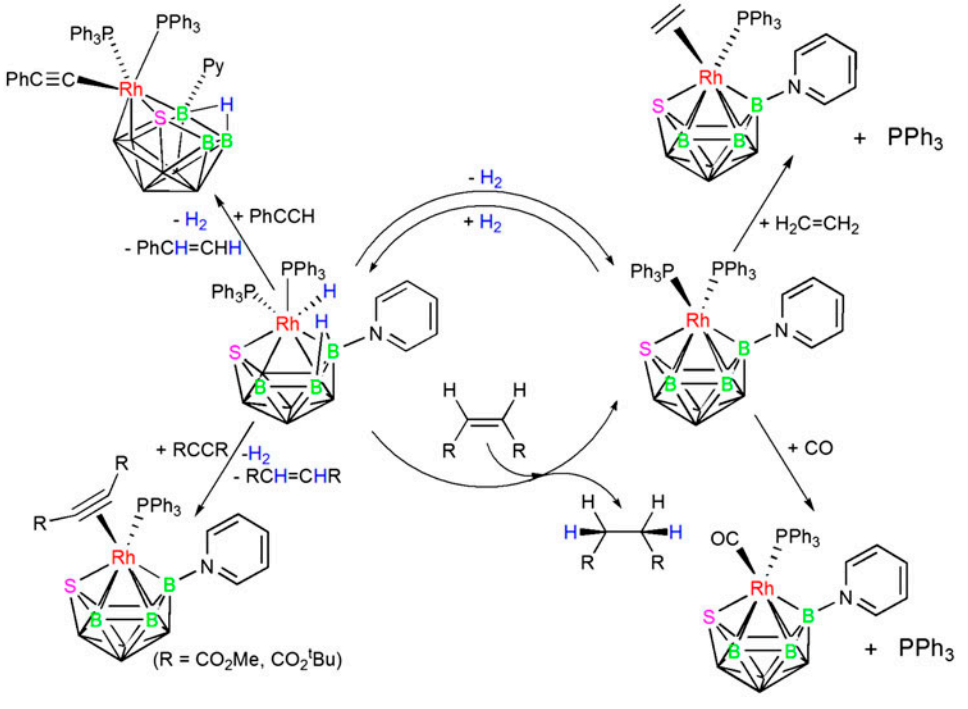

Scheme 1. Some reactions of [8,8,8-$(PPh_3)_2$H-9-(NC_5H_5)-*nido*-8,7-$RhSB_9H_9$].

incorporation of a hemilabile ligand such as nitrile has afforded species with a dangling C≡N coordinating moiety that has potential to coordinate to the rhodium center in an intramolecular fashion or, alternatively, to coordinate intermolecularly to form bimetallic species. These modes of coordination may improve the catalytic activity of this type of 11-vertex clusters through the stabilization of new intermediates that may perform better than the previously studied systems in, for example, hydrogenation of olefins [22].

2. Results and discussion

The reaction of [8,8-$(PPh_3)_2$-*nido*-8,7-$RhSB_9H_{10}$] (**1**) with 3-pyridineacetonitrile (3-Py-CH_2CN) under an argon atmosphere at room temperature yields orange solid [8,8,8-(H)$(PPh_3)_2$-9-(3-Py-CH_2CN)-*nido*-8,7-$RhSB_9H_9$] in 92% isolated yield (**2**, scheme 2).

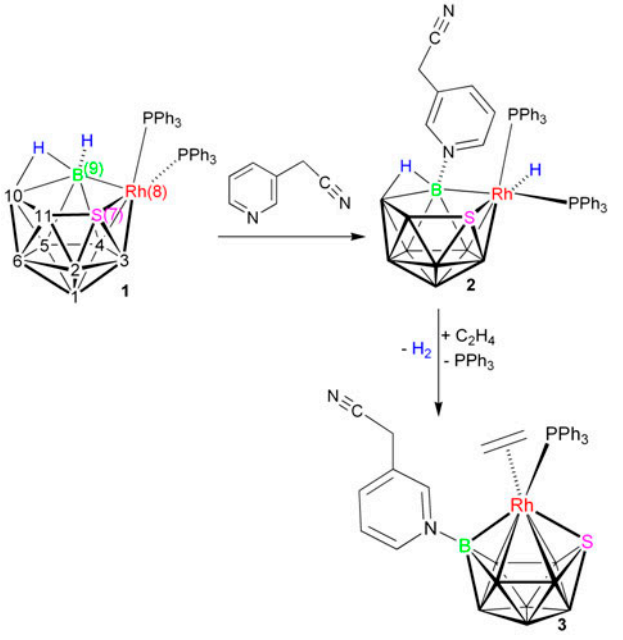

Scheme 2. Formation of [8,8,8-(H)$(PPh_3)_2$-9-(3-Py-CH_2CN)-*nido*-8,7-$RhSB_9H_9$] (**2**) and its reaction with ethylene to give [1,1-(η^2-C_2H_4)(PPh_3)-3-(3-Py-CH_2CN)-*closo*-1,2-$RhSB_9H_8$] (**3**).

In this reaction, the terminal hydrogen at the B(9) vertex adjacent to the metal center at position 8 is formally substituted by the N-heterocyclic reagent, 3-Py-CH_2CN (see scheme 2 for the cluster numbering). The detailed mechanism of this reaction is unknown at this time, although two possible reaction pathways may be envisioned: (a) the Lewis base directly attacks boron atom B(9), leading to the migration of the terminal hydrogen to the metal center, and (b) the incoming ligand coordinates the metal center and subsequently migrates to the B(9) vertex in a process that involves the concerted movement of the terminal hydrogen to the rhodium center (scheme 2). Alternatively, the B(9)–H–B(10) bridging hydrogen may be involved in both proposed concerted migrations instead of the terminal hydrogen atom, B(9)–H. Recently, we have demonstrated that the substitution reactions of **1** with monodentate phosphines follow an associative mechanism and, based on these results, it is therefore more probable that the formation of the hydridorhodathiaborane occurs via coordination of the incoming Lewis base to the metal center (scheme 3).

The 3-pyridylacetonitrile-ligated hydridorhodathiaborane, **2**, has been characterized by multielement NMR spectroscopy and mass spectrometry. This compound is sparingly soluble in dichloromethane, suggesting that the cluster may exhibit intermolecular interactions

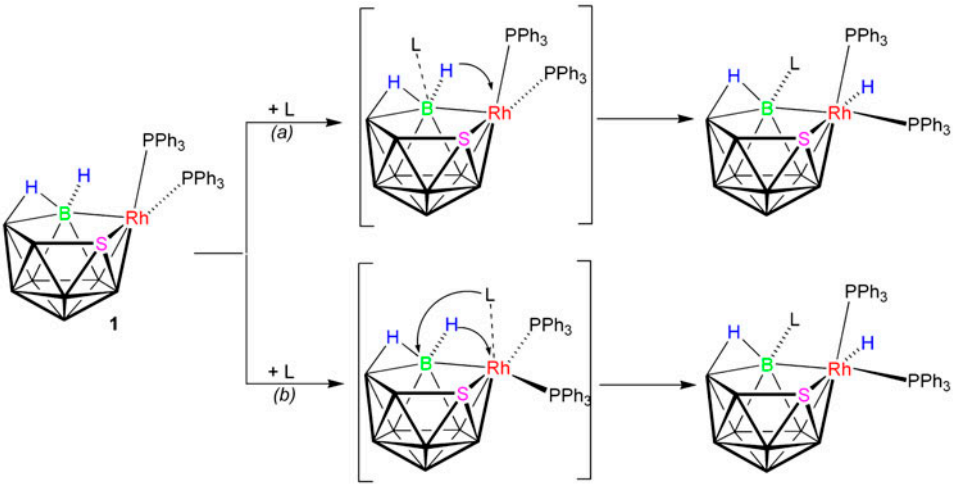

Scheme 3. Proposed pathways for the reaction of **1** with 3-Py-CH_2CN (L): (a) direct attack at the B(9) vertex and (b) attack mediated by the metal center.

leading to an extended association in the solid state. Unfortunately, we have not yet been able to grow a crystal suitable for single-crystal X-ray diffraction analysis.

The ^{11}B-{^1H} NMR spectrum exhibits nine resonances ranging between δ_B + 12.1 and −26.9 ppm, which is within the range found for pyridine- and picoline-ligated analogs, [8,8,8-(H)$(PPh_3)_2$-9-(L)-*nido*-8,7-$RhSB_9H_9$], where L = Py, 2-Me-Py, 3-Me-Py, and 4-Me-Py [27]. The highest frequency peak corresponds to the 3-pyridylacetonitrile-substituted boron as is found in the pyridine and picoline analogs.

The ^1H-{^{11}B} NMR spectrum of **2** shows a broad singlet and an apparent quartet in the high-field region, which may be assigned to the B(9)–B(10) bridging hydrogen atom and to the Rh–H hydride ligand, respectively. These spectroscopic data are diagnostic for this class of 11-vertex *nido*-hydridorhodathiaboranes.

The low-temperature ^{31}P-{^1H} spectrum of **2** exhibits two doublets-of-doublets with the resonance at highest frequency being much broader. This latter resonance increasingly broadens and shifts to lower frequency as the temperature is increased. The low-frequency signal moves to a slightly higher frequency. This variable temperature NMR behavior is similar to that found for the [8,8,8-(H)(PPh_3)-9-(L)-*nido*-8,7-$RhSB_9H_9$] analogs (where L = Py, 2-Me-Py, 3-Me-Py, and 4-Me-Py) [27].

It has been proposed that the temperature-dependent broadening in the ^{31}P-{^1H} spectra of N-heterocyclic-ligated hydridorhodathiaboranes may arise mainly from the effects of "thermal decoupling" of the boron nuclei [28] together with the dissociation of the phosphine ligand *trans* to B(9) [22, 23]. Using this rationale, the broader peak at high frequency, in this new family of 11-vertex hydrido-ligated clusters, may be assigned to the phosphine ligand that is *trans* to the Lewis base-substituted boron vertex at the 9-position.

Compound **2** reacts with ethylene to afford [1,1-(η^2-C_2H_4)(PPh_3)-3-(3-Py-CH_2CN)-1,2-$RhSB_9H_8$] (**3**) in 74% isolated yield, through 3-pyridylacetonitrile cage substitution and dihydrogen loss (*vide infra*), resulting in a cluster with a *closo*/*isonido*-electron count. This ethylene-ligated cluster has been characterized by multielement NMR spectroscopy and X-ray diffraction analysis. The ^{11}B NMR spectrum shows seven signals with a 1 : 1 : 2 : 1 : 1 : 1 : 2 relative intensity ratio in accord with an asymmetric cluster. The resonance at

δ_B + 55.4 ppm corresponds to the B(3)-substituted 3-pyridylacetonitrile vertex. At room temperature in the ^{1}H NMR spectrum, the ethylene ligand shows two signals that split into four peaks at low temperature. This variable temperature behavior demonstrates that the Rh-(η^2-C_2H_4) interaction is fluxional, undergoing a hindered rotation that renders the two C–H pairs equivalent. The free energy barrier, calculated at the coalesce temperature, for this rotational process is 11.7 kJ mol^{-1} (see Supplementary material). This is also the

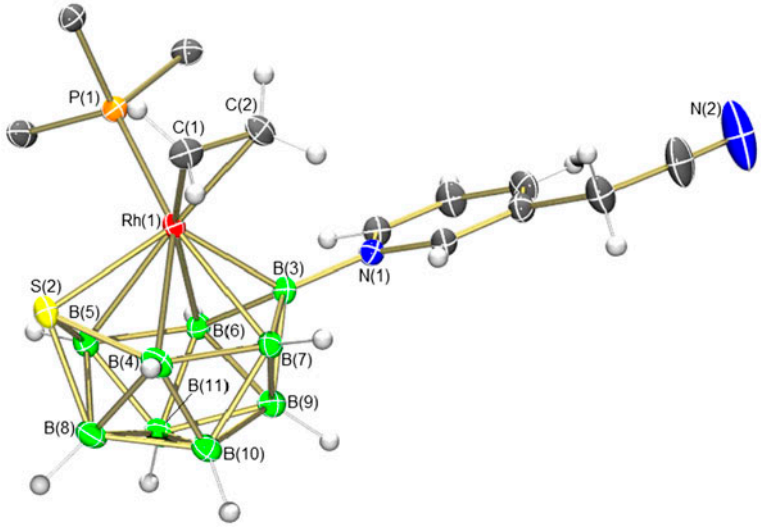

Figure 1. Crystallographically determined molecular structure of [1,1-(η^2-C_2H_4)(PPh_3)-3-(3-Py-CH_2CN)-*closo*-1,2-$RhSB_9H_8$] (**3**).

Table 1. Selected interatomic distances (Å) and angles (°) with Estimated Standard Uncertainties (s.u.) in parentheses for [1,1-(η^2-C_2H_4)(PPh_3)-3-(3-$NCCH_2$Py)-*closo*-1,3-$RhSB_9H_8$] (**3**) and [1,1-(η^2-C_2H_4)(PPh_3)-3-(Py)-*closo*-1,3-$RhSB_9H_8$] (**4**).

	3	**4** [22]
Rh(1)–S(2)	2.3615(7)	2.3721(9)
Rh(1)–P(1)	2.3000(7)	2.2981(9)
Rh(1)–C(1)	2.164(3)	2.165(3)
Rh(1)–C(2)	2.172(3)	2.171(4)
Rh(1)–B(3)	2.087(3)	2.079(4)
Rh(1)–B(4)	2.445(3)	2.427(4)
Rh(1)–B(5)	2.490(3)	2.503(4)
Rh(1)–B(6)	2.411(3)	2.365(4)
Rh(1)–B(7)	2.330(3)	2.376(4)
S(2)–B(4)	1.938(3)	1.948(4)
S(2)–B(5)	1.935(3)	1.929(4)
S(2)–B(8)	1.990(3)	1.985(4)
C(1)–C(2)	1.383(4)	1.383(5)
N(1)–B(3)	1.544(3)	1.539(5)
P(1)–Rh(1)–S(2)	103.81(2)	112.86(3)
P(1)–Rh(1)–B(3)	116.85(8)	109.13(11)
S(2)–Rh(1)–B(3)	119.34(8)	119.58(11)
Rh(1)–B(3)–N(1)	130.72(19)	127.7(2)
C(1)–Rh(1)–P(1)	95.84(8)	89.32(11)
C(2)–Rh(1)–P(1)	89.08(8)	93.39(10)

activation energy $\Delta G^{\ddagger}$ found for the full rotation of the ethylene ligand about the coordination bond in the pyridine-ligated analog, [1,1-(η^2-C_2H_4)(PPh_3)-3-(Py)-1,2-$RhSB_9H_8$] (**4**) [22].

Figure 1 depicts the molecular structure of **3** determined by X-ray diffraction, and table 1 lists selected distances and angles together with the values for the pyridine-ligated analog, [1,1-(η^2-C_2H_4)(PPh_3)-3-(Py)-1,2-$RhSB_9H_8$] (**4**) [22]. At first sight, the structure of the cluster is based on an octadecahedron. It should be noted that both the 3-pyridyl-acetonitrile and the pyridine derivatives feature long Rh(1)-B(5) distances close to 2.5 Å, which is the upper limit normally considered as bonding. This relatively long Rh(1)-B(5) linkage is *trans* to the η^2-ethylene ligand in both rhodathiaboranes, **3** and **4**. This type of elongation has been found in other 11-vertex metallaheteroboranes that exhibit a *pseudo*-square open face [29], which represent intermediates along the structural continuum from *closo* to *nido* [30–33].

In the crystal lattice, the clusters show intermolecular edge-to-face π-interactions. The observed C–H···C contacts are in the range 2.70–2.85 Å, being shorter than the v*an der Waals radii.* Each cluster shows three of these interactions with two adjacent neighbors (figure 2). It is noteworthy that these attractive π-forces lead to the placement of the B(7)

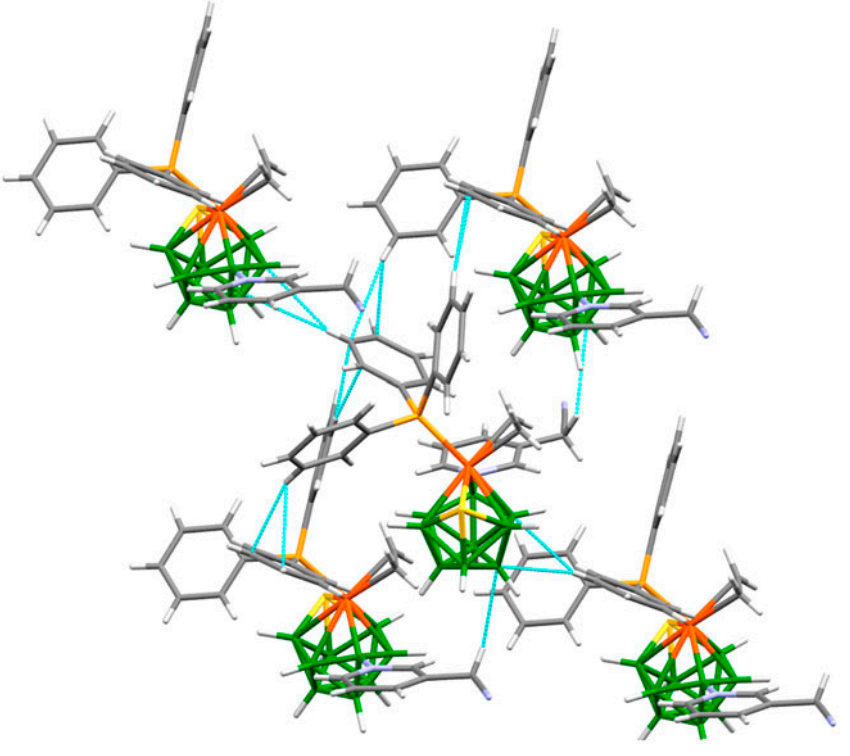

Figure 2. Section of the crystal structure of [1,1-(η^2-C_2H_4)(PPh_3)-3-(3-Py-CH_2CN)-*closo*-1,2-$RhSB_9H_8$] (**3**), showing the short contacts between the clusters. There are edge-to-face π-interactions between the phenyl rings ranging from 2.70 to 2.85 Å, and B···H–C distances at 2.97 and 3.13 Å between the C–H units of one phenyl rings and the B(7) and B(10) vertices, and between a C–H unit of the acetonitrile group and the B(10) vertex at 3.12 Å.

and B(10) vertices near C–H units of phenyl rings and the $–CH_2CN$ dangling groups of adjacent clusters. The result is the formation of chains that grow along the crystallographic *c*-axis. These chains pack on the *ac*-plane to form a layer, which self-assemble, via the commented π-interactions, with an adjacent parallel layer, forming an AB-type of a double layer. The repetition of this close-packed double layer in the unit cell forms the solid structure of **3** (figure 3).

It is interesting to note that the low-resolution mass spectra of **2** and **3** give an ion centered at *m/z* 979 with an isotopic pattern that matches a molecular ion with the formula, $[\{(PPh_3)(RhSB_9H_8)\}(3\text{-Py-}CH_2CN)\{3\text{-Py-}CH_2CN(RhSB_9H_8)\}]^+$ (see figures S1 and S2, see online supplemental material at http://dx.doi.org/10.1080/00958972.2014.959004). A reasonable interpretation is that this ion contains a $\{(PPh_3)(RhSB_9H_8)\}$ fragment and a $\{(3\text{-Py-}CH_2CN)(RhSB_9H_8)\}$ unit bridged by a 3-pyridyl ligand. In addition, the spectra show the fragmented ion $[(PPh_3)RhSB_9H_8(3\text{-Py-}CH_2CN)]^+$ at *m/z* 621 (figure 4). These results suggest that the dangling nitrile group in **2** and **3** can coordinate other metal centers leading to the formation of dimeric species:

$$2\left[(H)(PPh_3)_2RhSB_9H_9(3\text{-Py-}CH_2CN)\right]^{\bullet+} \rightarrow [\{(PPh_3)RhSB_9H_8\}(3\text{-Py-}CH_2CN)\{(3\text{-Py-}CH_2CN)RhSB_9H_8\}]^{\bullet+} + 4H + 3PPh_3$$

$$2[(C_2H_4)(PPh_3)RhSB_9H_8(3\text{-Py-}CH_2CN)]^{\bullet+} \rightarrow [\{(PPh_3)RhSB_9H_8\}(3\text{-Py-}CH_2CN)\{(3\text{-Py-}CH_2CN)RhSB_9H_8\}]^{\bullet+} + PPh_3 + 2C_2H_4$$

The observed fragmentation processes involve the loss of dihydrogen and one PPh_3 ligand from the hydridorhodathiaborane **2**, and the ethylene ligand from **3**:

$$\left[(H)(PPh_3)_2RhSB_9H_9(3\text{-Py-}CH_2CN)\right]^{\bullet+} \rightarrow \left[(PPh_3)RhSB_9H_8(3\text{-Py-}CH_2CN)\right]^{\bullet+} + 2H + PPh_3$$

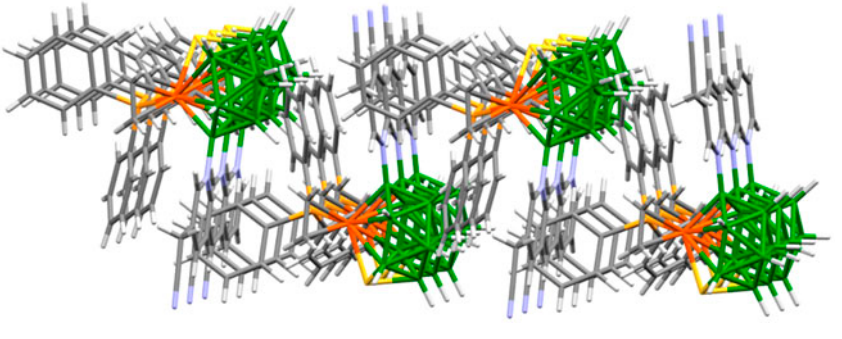

Figure 3. Packing of the crystal structure of $[1,1\text{-}(\eta^2\text{-}C_2H_4)(PPh_3)\text{-}3\text{-}(3\text{-Py-}CH_2CN)\text{-}closo\text{-}1,2\text{-}RhSB_9H_8]$ (**3**). View along the *c*-axis: the layers grow on the *ac*-plane.

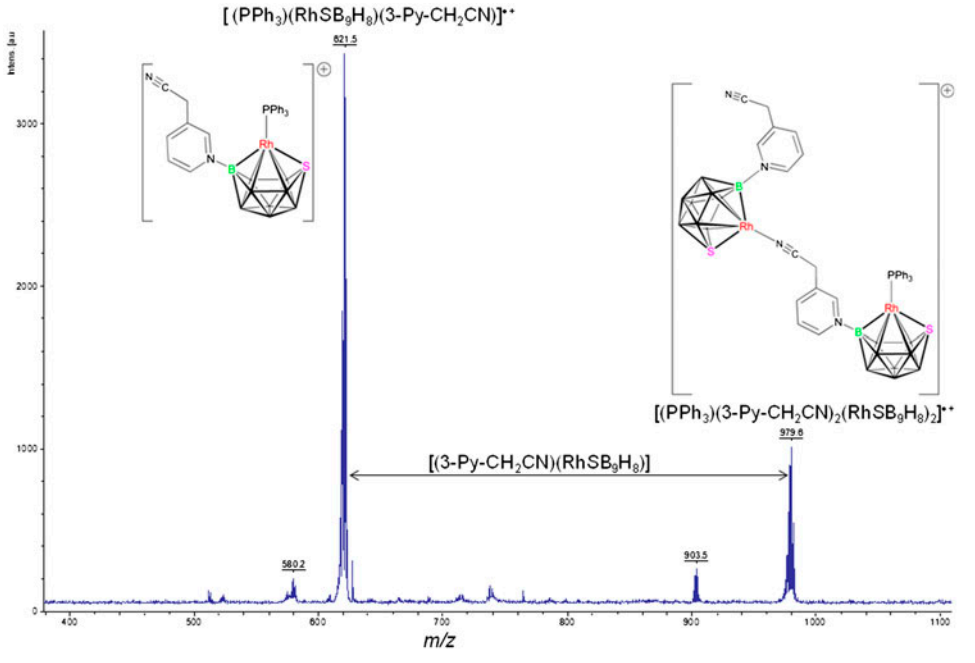

Figure 4. Positive ion LSMS spectrum of [1,1-(η^2-C_2H_4)(PPh_3)-3-(3-Py-CH_2CN)-*closo*-1,2-$RhSB_9H_8$] (**3**).

$$\left[(C_2H_4)(PPh_3)RhSB_9H_8(3\text{-Py-}CH_2CN)\right]^{\bullet+} \rightarrow \left[(PPh_3)RhSB_9H_8(3\text{-Py-}CH_2CN)\right]^{\bullet+} + C_2H_4$$

It should be noted that identical results were obtained using the matrices *trans*-2-[3-(4-*tert*-butylphenyl)-2-methyl-2-propenylidene]malononitrile (DCTB), terthiophene, and dithranol, suggesting that the formation of the dimeric ion is a fundamental property of these 3-pyridyl-ligated clusters.

3. Conclusion

Reaction of the 11-vertex rhodathiaborane **1** with 3-pyridylacetonitrile is a convenient method for the modification of the boron-bound *exo*-polyhedral ligands in 11-vertex rhodathiaboranes. The resulting labile hydridorhodathiaborane **2** reacts with ethylene to give an ethylene-ligated cluster, which has been characterized by X-ray diffraction analysis. This is only the second crystallographically determined ethylene-ligated polyhedral boron-based cluster reported in the literature.

The dangling nitrile group in **2** and **3** is open for the coordination to other metal centers; thus, both clusters are appropriate reagents for the potential synthesis of bimetallic systems.

In addition, the reaction of **3** with dihydrogen may afford unsaturated species, formed by the release of ethane, which could lead to intercluster coordination via the nitrile groups.

The incorporation of 3-pyridylacetonitrile on the 11-vertex *nido*- and *closo*-clusters is a straight-forward method for the modification of the *exo*-polyhedral surface of the clusters, thereby opening new possibilities for the coordination of different metals and leading to the development of their reaction chemistry.

4. Experimental

4.1. *General procedures*

Reactions were carried out under an argon atmosphere using standard Schlenk-line techniques. Solvents were obtained dried from a Solvent Purification System of Innovative Technology Inc. The 11-vertex rhodathiaborane **1** was prepared according to the literature methods [21]. NMR spectra were recorded on Bruker Avance 300-MHz and AV 400-MHz spectrometers using ^{31}P-{^{1}H}, ^{11}B, ^{11}B-{^{1}H}, ^{1}H, ^{1}H-{^{11}B}, and ^{1}H-{^{11}B(selective)} techniques. Residual solvent protons were used as reference (δ, ppm, $CDCl_3$, 7.26; CD_2Cl_2, 5.33; CD_3CN, 1.96). ^{11}B chemical shifts are quoted relative to $[BF_3(OEt)_2)]$, and ^{31}P chemical shifts are quoted relative to 85% aqueous H_3PO_4. Mass spectrometric data were recorded on a MICROFLEX instrument operating in the positive mode using matrix-assisted laser desorption ionization (MALDI). A nitrogen laser of 337 nm (photon energy of 3.68 eV) was used for the ionization processes, and the molecules under study were protected with three matrices: DCTB, dithranol and terthiophene.

4.2. *X-ray crystallography*

Crystals of **3** suitable for X-ray diffraction analysis were grown by slow diffusion of hexane into a concentrated solution of the rhodathiaborane in dichloromethane. X-ray diffraction data were collected at low temperature (100(2) K) on an automatic Bruker Kappa APEX DUO CCD area detector diffractometer equipped with graphite-monochromated Mo Kα radiation ($\lambda = 0.71073$ Å) using narrow frames (0.3° in ω). In all cases, single crystals were mounted on a fiber and were covered with a protective perfluoropolyether. Intensities were integrated including Lorentz and polarization effects with SAINT-Plus program [34] and corrected for absorption using multiscan methods applied with SADABS [35]. The structures were solved using the SHELXS-97 program [36]. Refinements were carried out by full-matrix least-squares on F^2 with SHELXL-97 [37], including isotropic and subsequent anisotropic displacement parameters for all non-hydrogen atoms. Experimental diffraction parameters and crystal data are gathered in table 2.

4.3. *Synthesis and NMR data*

4.3.1. [8,8,8-(H)(PPh_3)-9-(3-Py-CH_2-CN)-*nido*-8,7-$RhSB_9H_9$] (2). In a Schlenk tube, 116 mg (0.151 mmol) of **1** was dissolved in 10 mL of CH_2Cl_2, resulting in a bright-red solution. 160 μL (179 mg, 1.51 mmol) of 3-pyridylacetonitrile (3-Py-CH_2CN) was syringed into the solution, and the reaction mixture was stirred at room temperature for 7 h. After

Table 2. Crystallographic data and structure refinement information for [1,1-(η^2-C_2H_4)(PPh_3)-3-(3-Py-CH_2CN)-*closo*-1,2-$RhSB_9H_8$] (compound **3**).

Chemical formula	$C_{27}H_{33}B_9N_2PRhS$
Formula Mass	648.82
Crystal system	Monoclinic
a (Å)	11.1218(8)
b (Å)	21.6719(15)
c (Å)	13.8727(10)
α (°)	90.00
β (°)	113.3086(10)
γ (°)	90.00
Unit cell volume (Å^3)	3070.9(4)
Temperature (K)	100(2)
Space group	*P21/n*
No. of formula units per unit cell (Z)	4
Radiation type	Mo Kα
Absorption coefficient μ (mm^{-1})	0.698
No. of reflections measured	33287
No. of independent reflections	8019
R_{int}	0.0612
Final R_1 values ($I > 2\sigma(I)$)	0.0371
Final $wR(F^2)$ values ($I > 2\sigma(I)$)	0.0711
Final R_1 values (all data)	0.0687
Final $wR(F^2)$ values (all data)	0.0805
Goodness-of-fit on F^2	1.010

this time, the solvent was evaporated to dryness and the solid residue was washed three times with hexane. The final product was characterized as **2**. Yield: 100.8 mg, 0.139 mM, 92%. IR (ATR): ν 2535vs (BH), 2511vs (BH), 2460vs (BH), 2255w (CN), and 2060m (RhH). ^{11}B-{^{1}H} NMR (128 MHz; CD_2Cl_2; 298 K): δ + 12.1, +7.8, +3.5, +0.3, −3.8, −9.9, −18.5, −25.6, and −29.6. ^{1}H NMR (500 MHz; CD_2Cl_2; 298 K): δ + 7.91 (1H, br, 3-PyCH_2CN), +7.82 (1H, br, 3-PyCH_2CN), +7.35 – +7.05 (aromatics, PPh_3), +4.04 (v br, BH), +3.67 (ABq, 1H, $\Delta\nu_{AB}$ = 30.8 Hz, J_{AB} = 19.2 Hz, CH_2CN), +3.55 (ABq, CH_2CN), +2.85 (v br, BH), +1.84 (v br, BH), −1.37 (br s, BHB), and −12.51 (apparent q, J = 18.9 Hz, RhH); due to the insolubility of the compound, the terminal B–H peaks could not be observed. ^{31}P-{^{1}H} NMR (121 MHz; CD_2Cl_2; 213 K): δ + 36.3 (dd, J_{RhP} = 104.1 Hz) and + 30.4 (dd, J_{RhP} = 127.1 Hz, $^2J_{PP}$ = 19 Hz). LRMS (MALDI$^+$/DCTB): *m/z* [2M-3(PPh_3)-4H]$^+$ obsvd 979, Calcd for $P_1C_{32}H_{43}Rh_2S_2B_{18}N_4$: 979; [M-$PPh_3$-2H]$^+$ obsvd 621, Calcd for $P_1C_{25}H_{29}Rh_1S_1B_9N_2$: 621. The obsvd isotope envelope matches that calculated from the known isotopic abundances of the constituent elements.

4.3.2. [1,1-(PPh_3)(η^2-C_2H_4)-3-(3-Py-CH_2CN)-*closo*-1,2-$RhSB_9H_8$] (3). Fifty milligrams (0.056 mmol) of [8,8,8-(H)(PPh_3)-9-(3-Py-CH_2-CN)-*nido*-8,7-$RhSB_9H_9$] (**2**) was dissolved in 10 mL of CH_2Cl_2 in a Schlenk tube. After three freeze-thaw cycles, a balloon containing ethylene was attached to the Schlenk tube, and the rhodathiaborane solution exposed to the gas. The system was stirred at room temperature for 24 h and then concentrated by solvent evaporation under vacuum, after which hexane was added to produce an orange-red precipitate, which was then washed several times with hexane. The solid was crystallized from CH_2Cl_2/hexane to isolate the respective ethylene-ligated cluster, [1,1-(η^2-C_2H_4)(PPh_3)-3-(3-Py-CH_2CN)-*closo*-1,2-$RhSB_9H_8$]. Yield: 27 mg, 0.042 mmol, 74%. IR (ATR): ν 2529vs

(BH) and 2509vs (BH). ^{11}B-{^{1}H} NMR (96 MHz, $CDCl_3$, 298 K): δ + 55.4 (s, B–N), +26.2 (s, BH, $^{1}J(^{11}\text{B}\text{-}^{1}\text{H})$ = 122 Hz), +1.1 (s, 2B-H), −14.2 (s, B–H), −21.9 (s, B–H, $^{1}J(^{11}\text{B}\text{-}^{1}\text{H})$ = 128 Hz), −24.5 (s, B–H, $^{1}J(^{11}\text{B}\text{-}^{1}\text{H})$ = 126 Hz), and −29.8 (s, 2B-H). ^{1}H-{^{11}B} NMR (300 MHz, $CDCl_3$, 298 K): δ + 9.30 (1H, br, 3-PyCH_2CN), +9.19 (1H, br, 3-PyCH_2CN), +8.35 (1H, br, 3-PyCH_2CN), +7.84 (1H, br, 3-PyCH_2CN), +4.22 (s, B–H), +3.94 (ABq, 1H, $\Delta\nu_{AB}$ = 27.5 Hz, J_{AB} = 18.5 Hz, CH_2CN), +3.81 (ABq, CH_2CN), +2.27 (s, B–H), +2.28 (C_2H_4), +2.09 (C_2H_4), +1.96 (s, B–H), +1.60 (s, B–H), +0.43 (s, B–H), +0.22 (s, B–H), and −0.19 (s, B–H), −0.23 (s, B–H). ^{31}P-{^{1}H} NMR (121 MHz, $CDCl_3$, 298 K): δ + 39.0 (d, PPh_3, J_{RhP} = 141 Hz). LRMS (MALDI$^+$/DCTB): *m/z* [2M-(PPh_3)-2(C_2H_4)]$^+$ obsvd 979, Calcd for $P_1C_{32}H_{43}Rh_2S_2B_{18}N_4$: 979; [M-($C_2H_4$)]$^+$ obsvd 621, Calcd for $P_1C_{25}H_{29}Rh_1S_1B_9N_2$: 621. The obsvd isotope envelope matches that calculated from the known isotopic abundances of the constituent elements.

Supplementary material

CSD-CCDC 1006809 contains the supplementary crystallographic data for this article. Measured and calculated isotopic patterns for **2** and **3**.

Acknowledgments

We acknowledge the Spanish Ministry of Science and Innovation (CTQ2012-32095, CONSOLIDER INGENIO, CSD2009-00050, MULTICAT and CSD2006-0015, Crystallization Factory) for support of this work and the KFUPM-University of Zaragoza research agreement. B.C. thanks the "Diputación General de Aragón" for a pre-doctoral scholarship.

References

[1] R.N. Grimes. In *Comprehensive Organometallic Chemistry*, G. Wilkinson, F.G.A. Stone, E.W. Abel (Eds), pp. 459–542, Pergamon, Oxford (1982).
[2] R. Grimes. In *Metal Interactions with Boron Clusters*, R. Grimes (Ed.), pp. 269–319, Springer, New York, NY (1982).
[3] R.N. Grimes. *Chem. Rev.*, **92**, 251 (1992).
[4] R.N. Grimes. In *Comprehensive Organometallic Chemistry II*, E.W. Abel, F.G.A. Stone, G. Wilkinson (Eds), pp. 373–430, Pergamon, Oxford (1995).
[5] T.D. McGrath, F.G.A. Stone. *Adv. Organomet. Chem.*, **53**, (2005).
[6] B.E. Hodson, T.D. McGrath, F.G.A. Stone. *Organometallics*, **24**, 1638 (2005).
[7] T.D. McGrath, F.G.A. Stone. *J. Organomet. Chem.*, **689**, 3891 (2004).
[8] D.D. Ellis, P.A. Jelliss, F.G.A. Stone. *Spec. Publ. - R. Soc. Chem.*, **253**, 291 (2000).
[9] P.A. Jelliss, F.G.A. Stone. *J. Organomet. Chem.*, **500**, 307 (1995).
[10] S.A. Brew, F.G.A. Stone. *Adv. Organomet. Chem.*, **35**, 135 (1993).
[11] F.G.A. Stone. *Adv. Organomet. Chem.*, **31**, 53 (1990).
[12] A.K. Saxena, J.A. Maguire, N.S. Hosmane. *Chem. Rev.*, **97**, 2421 (1997).
[13] A.K. Saxena, N.S. Hosmane. *Chem. Rev.*, **93**, 1081 (1993).
[14] J.D. Kennedy. *Prog. Inorg. Chem.*, **34**, 211 (1986).
[15] J.D. Kennedy. *Prog. Inorg. Chem.*, **32**, 519 (1984).
[16] L. Barton, D.K. Srivastava. In *Comprehensive Organometallic Chemistry II*, E.W. Abel, F.G.A. Stone, G. Wilkinson (Eds), pp. 275–372, Pergamon, New York (1995).
[17] L.T. Todd. In *Comprehensive Organometallic Chemistry II*, E.W. Abel, F.G.A. Stone, G. Wilkinson (Eds), pp. 257–273, Elsevier Science, Oxford (1995).

[18] L.T. Todd. In *Comprehensive Organometallic Chemistry*, G. Wilkinson, F.G.A. Stone, E.W. Abel (Eds), pp. 534–553, Pergamon, Oxford (1982).
[19] L. Wesemann. In *Comprehensive Organometallic Chemistry*, D.M.P. Mingos, R.H. Crabtree (Eds), pp. 113–131, Elsevier, Oxford (2007).
[20] A.S. Weller. In *Comprehensive Organometallic Chemistry III*, R.H. Crabtree, D.M.P. Mingos (Eds), pp. 133–174, Elsevier, Oxford (2007).
[21] G. Ferguson, M.C. Jennings, A.J. Lough, S. Coughlan, T.R. Spalding, J.D. Kennedy, X.L.R. Fontaine, B. Stibr. *J. Chem. Soc., Chem. Commun.*, 891 (1990).
[22] Á. Álvarez, R. Macías, J. Bould, M.J. Fabra, F.J. Lahoz, L.A. Oro. *J. Am. Chem. Soc.*, **130**, 2148 (2008).
[23] Á. Álvarez, R. Macías, J. Bould, M.J. Fabra, F.J. Lahoz, L.A. Oro. *J. Am. Chem. Soc.*, **130**, 11455 (2008).
[24] B. Calvo, R. Macías, V. Polo, M.J. Artigas, F.J. Lahoz, L.A. Oro. *Chem. Commun.*, **49**, 9863 (2013).
[25] Á. Álvarez, R. Macías, J. Bould, C. Cunchillos, F.J. Lahoz, L.A. Oro. *Chem. Eur. J.*, **15**, 5428 (2009).
[26] B. Calvo, R. Macías, M.J. Artigas, F.J. Lahoz, L.A. Oro. *Chem. Eur. J.*, **19**, 3905 (2013).
[27] Á. Álvarez, B. Calvo, R. Macías, F.J. Lahoz, L.A. Oro. *Organometallics*, **33**, 3137 (2014).
[28] H. Beall, C.H. Bushweller, W.J. Dewkett, M. Grace. *J. Am. Chem. Soc.*, **92**, 3484 (1970).
[29] E.G. Kononova, L.A. Leites, S.S. Bukalov, I.V. Pisareva, I.T. Chizhevsky, J.D. Kennedy, J. Bould. *Eur. J. Inorg. Chem.*, 4911 (2007).
[30] K. Nestor, X.L.R. Fontaine, N.N. Greenwood, J.D. Kennedy, J. Plesek, B. Stibr, M. Thornton-Pett. *Inorg. Chem.*, **28**, 2219 (1989).
[31] M. Bown, X.L.R. Fontaine, N.N. Greenwood, J.D. Kennedy, M. Thornton-Pett. *Organometallics*, **6**, 2254 (1987).
[32] K. Nestor, X.L.R. Fontaine, N.N. Greenwood, J.D. Kennedy, M. Thornton-Pett. *J. Chem. Soc., Chem. Commun.*, 455 (1989).
[33] J. Bould, C. Cunchillos, F.J. Lahoz, L.A. Oro, J.D. Kennedy, R. Macías. *Inorg. Chem.*, **49**, 7353 (2010).
[34] Bruker, *SAINT-PLUS (Version 6.01)*, Bruker AXS Inc, Madison, WI (2001).
[35] G.M. Sheldrick. *SADABS*, University of Göttingen, Göttingen (1999).
[36] G.M. Sheldrick. *Acta Crystallogr.*, **46**, 467 (1990).
[37] G.M. Sheldrick. *Acta Crystallogr.*, **64**, 112 (2008).